Convective Influence on the Heat Balance of the Tropical Tropopause Layer: A Cloud-Resolving Model Study

ZHIMING KUANG AND CHRISTOPHER S. BRETHERTON

Department of Atmospheric Sciences, University of Washington, Seattle, Washington

(Manuscript received 1 March 2004, in final form 2 June 2004)

ABSTRACT

The tropical tropopause layer (TTL), and in particular the cold point tropopause, has been previously suggested as a feature decoupled from convection. Using a cloud-resolving model, the authors demonstrate that convection, in fact, has a cooling effect in the TTL that significantly affects its thermal structure. In particular, the cold point is found to be strongly tied to the convective cooling maximum. The authors interpret these as natural features of an entrainment layer such as the TTL. The recognition that the cold point tropopause is strongly tied to, rather than decoupled from, convection suggests that dehydration processes at the cold point cannot be assumed as gradual and the effect of convection may not be ignored.

1. Introduction

The transitional region between the tropical troposphere and stratosphere, or the tropical tropopause layer (TTL), has received considerable attention recently. Since the Brewer–Dobson circulation draws tropospheric air into the stratosphere mostly through the TTL, processes in this region exert important controls over stratospheric humidity, which affects stratospheric radiation, chemistry, and potentially the tropospheric climate as well (Kley et al. 2000).

Consensus is yet to be reached on some basic questions about the TTL, such as what determines its thermal structure, in particular, its temperature minimum (the cold point temperature). The cold point temperature warrants special attention because of its potential role in setting the stratospheric entry humidity (e.g., Holton and Gettelman 2001). Motivated by observations that most convection reaches no higher than ~200–150 hPa (Gettelman et al. 2002), Thuburn and Craig (2002) considered the cold point as a stratospheric feature decoupled from convection. Based on a 1D column radiative–convective equilibrium (RCE) model, they showed that a temperature minimum solely in radiative equilibrium can exist well above the convectively adjusted region, suggesting no direct role of convection on the cold point temperature. It is not clear, however, how applicable these results are to the real atmosphere. The 1D model assumes a discrete boundary between the convectively adjusted region and the radiative equilibrium region, while in nature the transition is known to be more gradual.

Although convective events that reach the TTL are admittedly infrequent, their effects on the heat budget may not be simply ignored. The long radiative relaxation time scale in the TTL allows small heating/cooling to induce substantial temperature changes. Using the radiative spring concept, one may express the effect of radiation as a damping term on temperature departures from radiative equilibrium, $\Delta T = T - T_{\mathrm{rad,eq}}$, and write the heat balance as

$$\Delta T/\tau = Q_c + Q_{\mathrm{l.s.}}, \tag{1}$$

where Q_c and $Q_{\mathrm{l.s.}}$ are the convective and large-scale heating, respectively, and τ is the radiative relaxation time scale ($Q_{\mathrm{l.s.}}$ will be introduced in section 3c). For τ on the order of 10 days, heating or cooling of a few tenths of a kelvin per day would be able to warm or cool the TTL by a few kelvin.

While observed cooling of the tropopause layer following convective events is largely adiabatic (Johnson and Kriete 1982), analyses of radiosonde data suggested that deep convective events may also induce diabatic cooling (Sherwood et al. 2003). However, the climatological effect of convection on the TTL thermal structure is not clear from such studies that focused on short time scales.

In this paper, we examine the heat balance in the TTL using a cloud-resolving model (CRM). Since a CRM resolves cumulus-scale motions, it is able to represent the decreasing, yet nonzero, convective influence in the TTL that is ignored in the 1D RCE study (Thuburn and Craig 2002). We shall focus on the basic issue of wheth-

Corresponding author address: Zhiming Kuang, Department of Atmospheric Sciences, University of Washington, Seattle, WA 98195-1640.
E-mail: kzm@atmos.washington.edu

er and how the inclusion of these relatively rare convective events may alter the conceptual picture of the TTL heat balance. For this purpose, we shall use RCE simulations with simplified settings, and exclude aspects of tropical atmosphere such as the large-scale circulation, mesoscale convective organizations, etc., both for computational practicality and for conceptual simplicity.

Section 2 contains a brief discussion of the model. We describe the experimental setup and present the results along with our interpretations in section 3. Section 4 summarizes the main results and discusses their implications.

2. Model

We use the System for Atmospheric Modeling (SAM), which is a new version of the Colorado State University Large Eddy Simulation/Cloud-Resolving Model (Khairoutdinov and Randall 2003). The model uses the anelastic equations of motion with bulk microphysics. The prognostic thermodynamic variables are the liquid water static energy, total nonprecipitating water, and total precipitating water. The longwave and shortwave schemes are those of the National Center for Atmospheric Research (NCAR) Community Climate Model, version 3 (CCM3; Kiehl et al. 1998). Readers are referred to Khairoutdinov and Randall (2003) for details about the model. For this study, we use a simple Smagorinsky-type subgrid-scale scheme. Similar to Tompkins and Craig (1998), we have removed the diurnal cycle by reducing the solar constant to 683.5 W m^{-2} and fixing the solar zenith angle at 50.5°. The surface fluxes are computed using Monin–Obukhov similarity.

3. Experiments, results, and discussion

a. Control experiment setup

As a control run, we use a doubly periodic domain of 64 km × 64 km with the model top placed near 40 km. The horizontal grid size is uniformly 1 km. In our simulations, we find that convection is able to occur continuously somewhere in the domain. We take this as an indication that our domain size is sufficiently large to not overly constrain the behavior of the convective ensembles, following suggestions of Tompkins and Craig (1998). To simplify the heat budget in the TTL, we use a zero background wind profile to discourage gravity wave breaking. We use stretched vertical grids, with a total of 144 grid points, as shown in Fig. 1. A wave-absorbing layer was placed in the upper third of the domain. The vertical grid size decreases above ~14 km and reaches 100 m in the lower stratosphere. This is roughly proportional to the inverse of the local buoyancy frequency, and was so designed to reduce artificial gravity wave damping. Since the buoyancy frequency increases from the upper troposphere to the height of maximum static stability (~18–19 km) by a factor of 4–5 [estimated from the mean Tropical Ocean Global Atmosphere Coupled Ocean–Atmosphere Response Experiment (TOGA COARE) soundings; Webster and Lukas (1992)], upward-propagating gravity waves generated in the upper troposphere become increasingly compressed in their vertical scale. Without a corresponding decrease in the vertical grid size, these waves become more and more poorly resolved and hence prone to numerical dissipation. While for inviscid gravity waves, buoyancy and vertical velocity perturbations are 90° out of phase so that the net buoyancy flux (or heat flux as the amount of water is small in the TTL) is zero, when wave dissipation is included, the phase difference between buoyancy and vertical velocity perturbations is modified to yield downward heat fluxes (Matcheva and Strobel 1999). Numerical dissipation of these waves can therefore cause artificial cooling/heating. We found that this effect was largely removed with our choice of vertical grid layout.

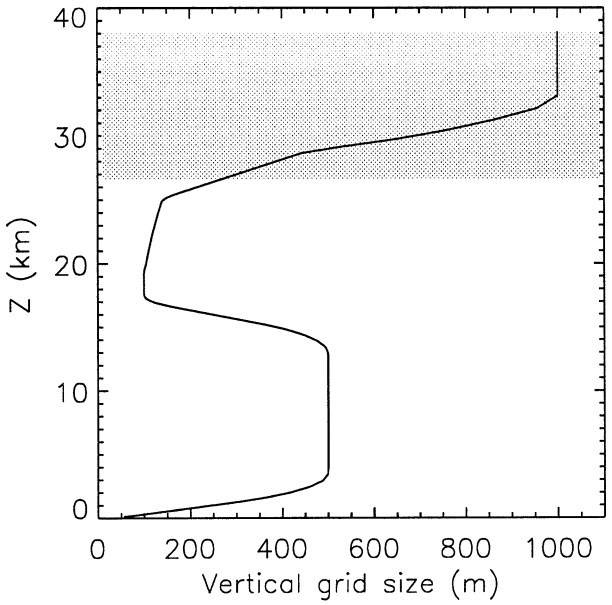

FIG. 1. Vertical grid size as a function of height. The shaded region represents the wave-absorbing layer.

For this study, the ozone profile is specified to be the mean profile of the TOGA COARE for December 1992 and January 1993 (Webster and Lukas 1992). In nature, convection could affect radiation by changing the ozone field in the TTL. In this work, however, we shall focus on the direct thermal effect of convection and ignore the effect of convection on the ozone profile. Water vapor in the stratosphere is specified in the initial condition to increase from 4 ppmv near 100 hPa to 6 ppmv at the top of the domain because it is essentially unchanged during the simulation. The results in the TTL are not sensitive to this specification. The sea surface temperature (SST) is fixed to be uniformly 30.5°C. Due to the lack of background surface winds, this rather high

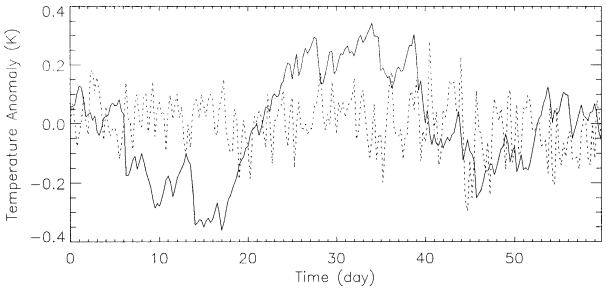

FIG. 2. Domain-averaged temperature fluctuations at the cold point (solid) and at 6 km (dotted) over a 60-day period of the control simulation. The values are sampled every 5 min and 6-h averages are shown.

SST provides sufficient surface fluxes to give a surface air temperature of 27.5°C and a surface water mixing ratio of about 18 g kg^{-1}, similar to those observed over the western Pacific warm pool. We then run the model to RCE (which typically takes ~100 days), and examine the equilibrium heat balance.

We note that in the CRM simulations, the RCE achieved is a statistical equilibrium where temperature continues to fluctuate. The fluctuation is most pronounced at the cold point with periods of roughly 30 days and peak-to-valley differences of nearly 1 K (solid line in Fig. 2). This may be understood as the reddened response of a damped system (with a damping time scale of 20–30 days) to stochastic convective cooling [see Eq. (1)]. In contrast, temperatures in the bulk troposphere fluctuate with a much shorter time scale (dotted line in Fig. 2).

b. Heat balance in the control experiment

Figure 3 shows the heat balance from the control run. The heating/cooling rates are sampled every 5 min and averaged over a period of 50 days after RCE is achieved. (This applies to the later figures unless explicitly stated otherwise.) The convective heating is computed as the nonradiative portion of the liquid water static energy tendency. This includes subgrid-scale contributions, although they are generally small, and are negligible in the TTL. While in the bulk troposphere the heat balance is between convective heating and radiative cooling, near the tropopause (13–17 km) there is convective cooling balanced by radiative heating. The ripples above 17 km are sensitive to grid spacing of the model and therefore are nonrobust features due presumably to numerical dissipation.

To check the effect of resolution on the results, we repeated the experiment with doubled horizontal and vertical resolutions. The fine-resolution run is initiated with the RCE temperature and water profiles from the control experiment. Because of the high computational cost, the high-resolution experiment was run for only 20 days. It, nevertheless, confirms convective cooling and radiative heating in the TTL (not shown).

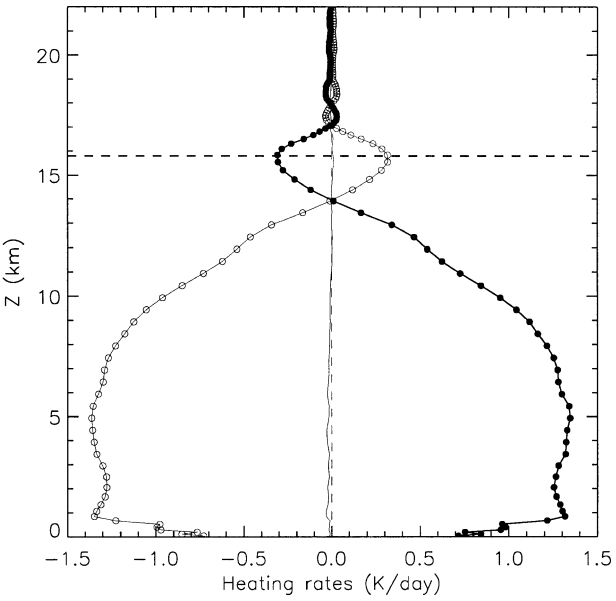

FIG. 3. Heating rates in the control experiment due to convection (filled circles) and radiation (open circles). Each circle represents one model level. The dashed horizontal line marks the cold point tropopause height. The solid vertical curve is the residual temperature tendency.

Potential nonradiative diabatic effects in the TTL include gravity wave breaking and direct injection of boundary layer air by penetrative convection. As we already mentioned, as convective updrafts oscillate around their levels of neutral buoyancy (LNB), they excite gravity waves that propagate into the stratosphere. As gravity wave breaking or damping induces downward heat fluxes, a nonuniform breaking/damping pattern in the TTL can introduce heat flux divergence/convergence, and hence cooling/heating. However, gravity waves generated by convection typically have amplitudes too small to break in the TTL unless they encounter a critical level, which requires strong wind shear. Our choice of zero background wind shear therefore strongly discourages the breaking of gravity waves in the TTL. Indeed, by inspection of the potential temperature field, we did not find evidence for gravity wave breaking. The lack of gravity wave breaking was also noted in a previous CRM study with weak background wind shear (Lane et al. 2003). Some damping of these gravity waves is nevertheless expected in the TTL through, for example, radiative relaxation. This damping, however, is rather uniform with height, and does not contribute significantly to the heat flux divergence.

Examination of individual convective events indicates that convective cooling is associated with the injection of boundary layer air. In Fig. 4, we show the domain-averaged temperature anomalies, boundary layer tracer concentrations, and cloud ice mass mixing ratios at the cold point tropopause for a period of 20 days.

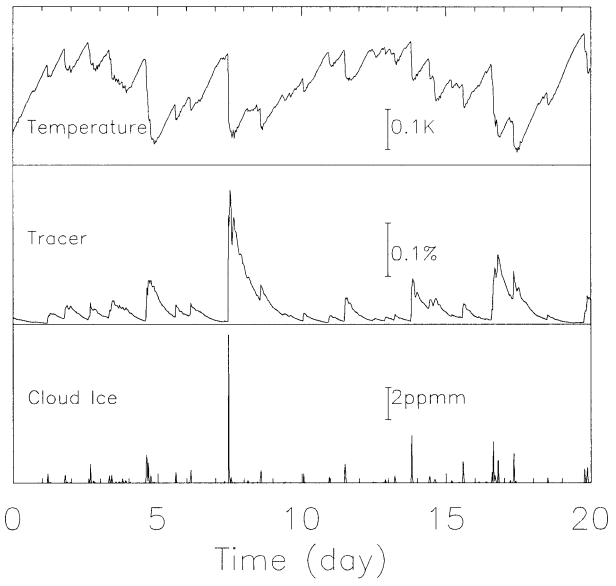

FIG. 4. Domain-averaged temperature anomalies, tracer concentrations, and cloud ice concentrations at the mean cold point tropopause level over a 20-day period of the control experiment. The values are sampled every minute and 30-min averages are shown. The cold point temperature drift over this period has been removed as a linear trend (see text for more explanation).

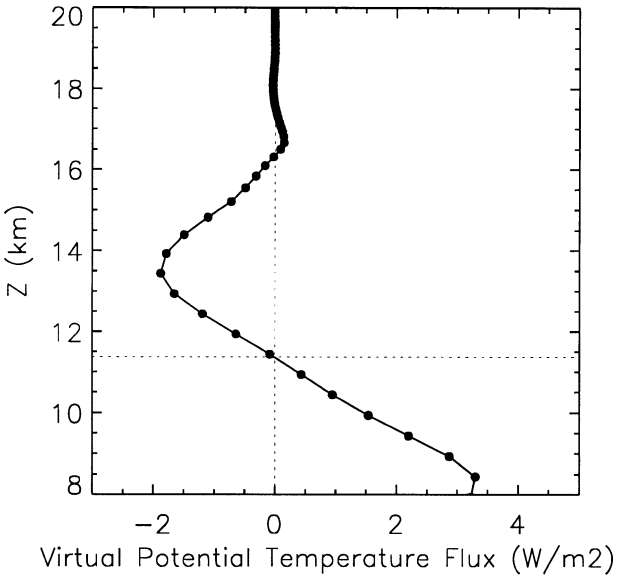

FIG. 5. Virtual potential temperature flux in energy flux units $\rho C_p \overline{w'\theta_v'}$. The horizontal line marks the LNB.

In this plot, the variables are sampled every minute and 30-min averages are shown.

To focus on the effect of individual events, the drift in the cold point temperature over this period has been removed in Fig. 4 as a linear trend. The tracer concentrations are set to unity every step in the lowest 600 m of the domain, and decay exponentially with a lifetime of 12 h outside of the boundary layer. Increases in the tracer concentration are thus indicative of injection of boundary layer air by deep convection. These events are accompanied by an increase of cloud ice, and a decrease in the cold point tropopause temperature. In the anelastic framework of SAM (Khairoutdinov and Randall 2003), when contributions from water substance can be neglected (a good approximation in the TTL), horizontally averaged temperature at a given height can be modified only by diabatic processes. The close correspondence between temperature drop and boundary layer tracer increase in Fig. 4 therefore shows the diabatic cooling of cold point tropopause by deep convection through injection of boundary layer air. Note also that cloud dissipates quickly after the convective events but temperature anomalies persist much longer. This occurs because removing a temperature anomaly by radiation near the cold point tropopause is a much slower process (20–30 days) than the dissipation of convective clouds (the time scale for the ice particles to fall out is on the order of hours). Thus the scarcity of convective clouds near the cold point tropopause does not imply the insignificance of convective influence on the heat balance. In fact, the mean cloud occurrence frequency (or time mean cloud fraction) at the cold point tropopause in this simulation is less than 0.5%, as rare as in the observations (Gettelman et al. 2002).

The existence of a convectively cooled region between a turbulent mixed layer and a stable layer is well documented in boundary layer studies (Deardorff et al. 1980). When a turbulent mixed layer is capped by an inversion, there is a transitional layer where fluid of the overlying stable layer is entraining but is not yet fully incorporated into the well-mixed turbulent layer. This layer is sometimes termed the entrainment layer. The TTL bears a direct resemblance to an entrainment layer, as it marks the transition between the troposphere, a turbulent mixed layer, and the stratosphere, a stable layer (Sherwood and Dessler 2001). In Fig. 5, we show the domain-averaged virtual potential temperature flux profile converted to energy flux units $\rho C_p \overline{w'\theta_v'}$, where ρ is density and C_p is the heat capacity at constant pressure. At TTL altitudes, the air is sufficiently dry so that virtual potential temperature flux, heat flux, and buoyancy flux have very similar profiles. Note the similarity between Fig. 5 and the heat flux profiles from convective water tank experiments (Deardorff et al. 1980). The region between where the heat flux first becomes negative (~11.4 km) and where the heat flux vanishes (~17 km) is the entrainment layer as defined in Deardorff et al. (1980). The shape of the heat flux in this region may be understood qualitatively by considering the downward convective heat flux as the product of the convective mass flux and the heat deficit of the convective mass relative to the environment. While the convective mass flux decreases with height above the LNB, because of the strong stratification in this region the heat deficit of the convective mass becomes increasingly large. The product of the two thus gives the shape in the TTL heat

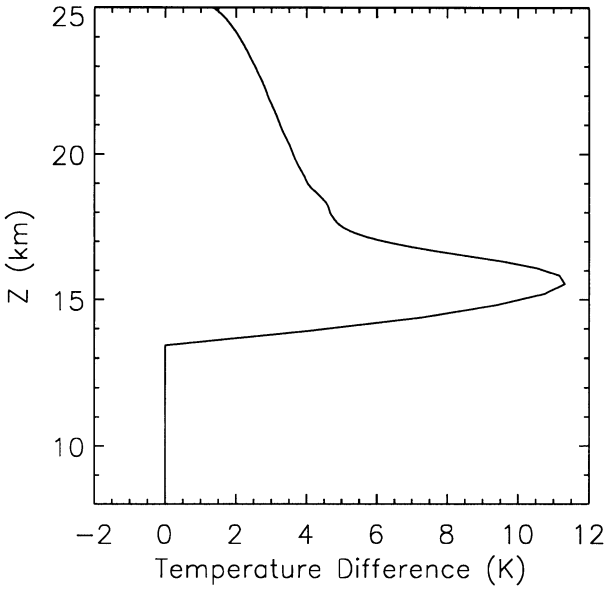

FIG. 6. Changes in the equilibrium TTL temperature when convective cooling is artificially removed.

flux. It also follows that above the level of most negative heat flux is a region of heat flux divergence, hence a region of convective cooling. [Note that in the literature, the LNB is sometimes taken as the same as the level of zero heating (Salby et al. 2003), while here we see that the level of zero heating is where the heat flux is most negative.] From these discussions, we conclude that the TTL in our control experiment behaves in ways similar to the entrainment layer in dry convective boundary layer experiments, and convective cooling from turbulent heat flux divergence in its upper portion is a natural feature of such an entrainment layer.

The magnitude of the convective cooling may be viewed as modest (a few tenths of a kelvin per day). However, due to the weak radiative spring in the TTL, this cooling significantly affects the temperature profile. To illustrate this, we did an experiment where convective cooling is artificially removed. Domain-averaged RCE profiles of water vapor, cloud, and temperature from the CRM experiment were used for the calculation. We held the temperature field below 13.5 km fixed and adjusted the temperature above until radiative equilibrium was achieved. The water vapor and cloud fields at all heights were kept unchanged from the CRM profiles. Figure 6 shows the difference between RCE temperature profile from the control experiment and the equilibrium temperature profile in the hypothetical experiment where convective cooling is removed. While the removal of convective cooling cannot be realized in nature, this experiment serves to show that a maximum of ~10 K cooling may be attributed to convective cooling at the cold point tropopause. This response, given the radiative heating of ~0.35 K day^{-1} at the cold point (Fig. 3), implies a radiative relaxation time scale of ~30 days, in line with some previous estimates (Hartmann et al. 2001). Note that the CRM cloud fields are used in the radiative calculations, so the temperature differences are not due to the radiative effects of thick anvil clouds. The temperature difference above 17 km is not due to convection directly. Rather, it is due to the fact that the new radiative equilibrium induces changes in temperature throughout the layer.

c. Effects of large-scale dynamical cooling

Let us now include the effect of mean upwelling on the heat balance in the tropical tropopause region. This is done by imposing a dynamical cooling term $w_{\text{l.s.}}(dh/dz)$ in the thermodynamic equation, where h is the liquid/ice water static energy. The prescribed large-scale vertical velocity, $w_{\text{l.s.}}$, is 0.3 mm s^{-1} in the stratosphere and gradually vanishes from 100 to 250 hPa, as suggested by the ''tape recorder'' observations (Mote et al. 1996). No large-scale vertical advection of the water vapor and ozone fields are included, however. This treatment is similar to that of Thuburn and Craig (2002). This experiment (hereafter w+3) is therefore more properly termed as an experiment with prescribed dynamical cooling rather than an experiment with prescribed vertical ascent. Results from this experiment are nevertheless comparable to the real tropical atmosphere because the stratospheric water and ozone profiles are prescribed with observed values that already included the effect of large-scale vertical advection.

The equilibrium temperature profile and the heat balance from experiment w+3 are shown in Fig. 7. The mean cold point is located at 16.8 km and the cold point temperature is 188 K, similar to the observed values over the west Pacific warm pool during Northern Hemisphere winter. In this more realistic experiment, convection is also found to cool the layer between ~14.3 and 18 km with a maximum rate of 0.2 K day^{-1}. At and below the cold point, dynamical and convective cooling rates are of similar magnitudes, while above the cold point, dynamical cooling becomes dominant.

d. Convective cooling and the cold point

An intriguing feature in Figs. 3 and 7 is that in both cases the cold point is located near the convective cooling maximum. This is in fact a robust feature in many other experiments. For instance, in Fig. 8, we show the heat balance in an experiment where the SST is increased by 2 K (hereafter SST+2) as compared to the control experiment. In this case, the cold point tropopause is ~600 m higher, but remains collocated with the convective cooling maximum. In other experiments where the SST is lowered by 2 K or a large-scale vertical advective heating is prescribed (the same vertical velocity profile as in w+3 was used except with the opposite sign), the two are also collocated (not shown).

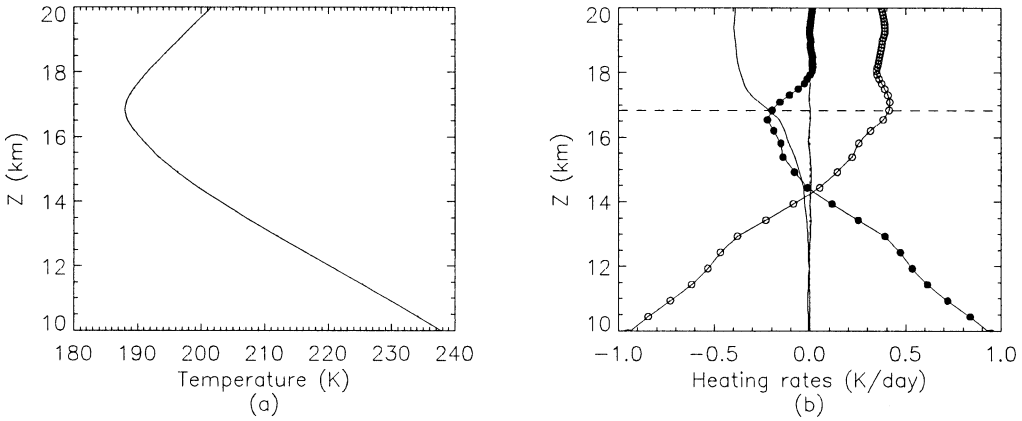

FIG. 7. Results from experiment w+3. (a) Equilibrium temperature profile. (b) Heating rates due to convection (filled circles), radiation (open circles), and large-scale advection (thick line). The dashed horizontal line in (b) marks the cold point height.

In general, there need be no fundamental connection between the cold point and convective cooling. For illustration purposes, let us consider a dry entrainment layer. The arguments apply equally well to the TTL owing to its small water content. As we have argued, convective cooling at the top of this entrainment layer is a natural feature of the entrainment dynamics, where potential temperature is the fundamental thermodynamic variable. Temperature, on the other hand, is merely a diagnostic variable related to potential temperature through the equation of state, and plays no direct role in the entrainment dynamics. For instance, for any finite stratification in the overlying stable layer, the entrainment layer, and hence the convective cooling, is expected to extend up to a finite height. On the other hand, if the stratification in the stable layer is sufficiently weak, in an atmosphere that obeys approximately the ideal gas law, the temperature will continuously decrease with height (dashed line in Fig. 9b). In this case, the cold point and the convective cooling maximum would not be close to each other.

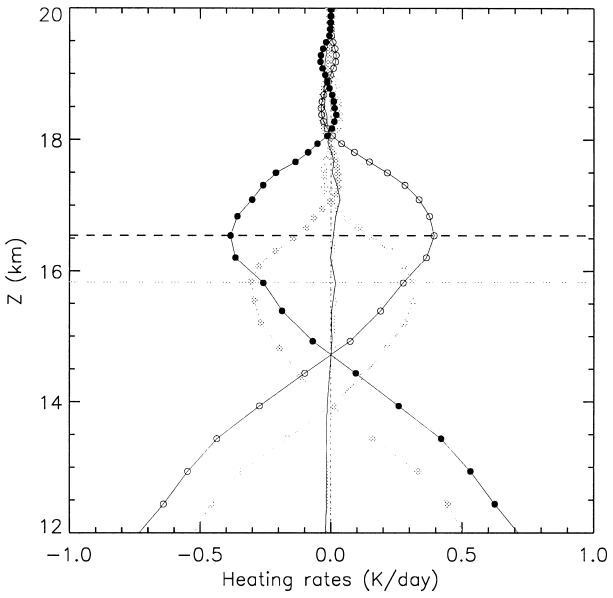

FIG. 8. Equilibrium heating rates from experiment SST+2 (dark lines) as compared to the control run (light lines). The symbols and the lines are the same as in Fig. 3.

When the stratification of the stable layer is sufficiently strong (solid lines in Fig. 9), however, the temperature minimum becomes closely related to the convective cooling maximum. Let us consider the RCE temperature profile as the result of perturbing the radiative equilibrium temperature with convective and large-scale cooling [Eq. (1)]. When the radiative equilibrium stratification in the upper portion of the entrainment layer is sufficiently strong, potential temperature increase with height overcomes the effect of pressure decrease so that vertical temperature gradient $dT_{\mathrm{rad,eq}}/dz$ changes sign. The upper portion of the entrainment layer is therefore a region of small $|dT_{\mathrm{rad,eq}}/dz|$. Because convective cooling has a peaked profile, combined with the long radiative relaxation time scale, it leaves a strong, peaked temperature perturbation, which in this case overlaps with a region of small $|dT_{\mathrm{rad,eq}}/dz|$. The location of the temperature minimum is therefore strongly determined by the convective cooling maximum.

The collocation between the cold point and the convective cooling maximum is of course affected by the large-scale dynamical cooling. Because of both the decreased ascent speed and the reduced static stability at lower altitudes, the large-scale dynamical cooling increases with height and therefore tends to ''pull'' the cold point upward and away from the convective cooling maximum. Some indication of this effect is seen in Fig. 7. For a sufficiently strong dynamical cooling, it is conceivable that the cold point would be eventually ''pulled'' out of the influence of convective cooling. For such a strong dynamical cooling, the stratification in the lower stratosphere would be greatly reduced to approach the weak stratification scenario illustrated in Fig. 9.

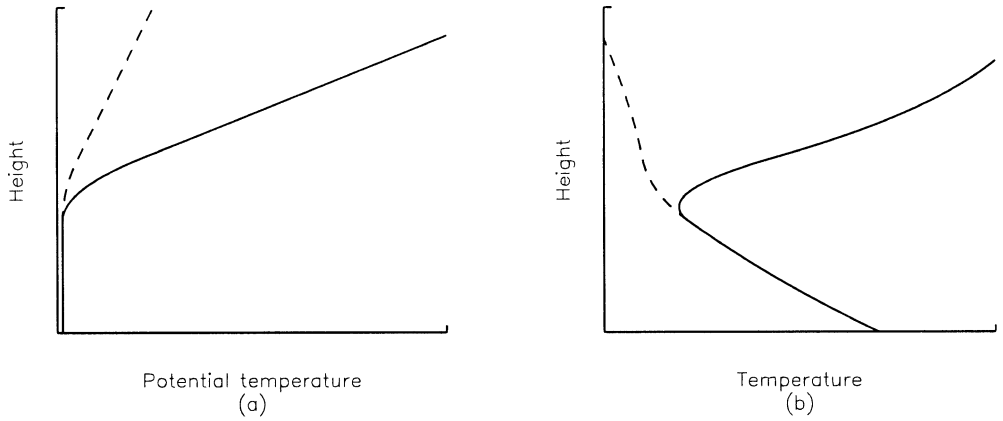

FIG. 9. Schematics of (a) potential temperature and (b) temperature profiles in a dry atmosphere with a well mixed lower layer capped by a weakly (dashed) or a strongly (solid) stratified stable layer. When the stratification is sufficiently weak, the temperature continuously decreases with height [dashed line in (b)].

Thus, in principle, it is possible for the cold point to be decoupled from convection as suggested by Thuburn and Craig (2002). However, since experiment w+3 produces a cold point tropopause height and temperature quite close to the observations (e.g., Folkins et al. 1999), the real atmosphere appears to fall under the scenario where the cold point remains close to the convective cooling maximum.

4. Summary and implications

The findings in this study may be summarized as the following:

1) The present model results support the view of the TTL as an entrainment layer. For an entrainment layer like the modeled TTL that is sufficiently dry so that buoyancy fluxes and heat fluxes are approximately the same (except for a proper conversion factor), cooling in its upper portion due to turbulent heat flux divergence is a natural feature.
2) Because of the long radiative time scale in the TTL (20–30 days), this cooling (a few tenths of a kelvin per day) has a large impact on the thermal structure.
3) While the cold point can in principle be decoupled from convection, the convective cooling maximum strongly determines where the cold point is when stratification in the upper part of the entrainment layer is sufficiently strong, a condition that appears to be satisfied by the real TTL.

Our findings contrast with those of a previous study using a 1D RCE model (Thuburn and Craig 2002), and highlight the need to consider the rare yet nonzero occurrence of deep convection that penetrates the TTL.

The simulations presented in this study are for an atmospheric column with active deep convection. When the atmosphere is organized into regions with and without deep convection, as in the real Tropics, convective cooling of the TTL experienced over the region with deep convection is expected to spread to the region without deep convection through wave propagation. Given the shallow cooling profile (see, e.g., Fig. 3), these waves would have slower propagation speeds as compared to the waves excited by the deep convective heating in the bulk troposphere. However, they may nevertheless be able to spread the cooling over a substantial distance, owing to the slow radiative damping process in the TTL. More studies, however, are needed to further elucidate these processes.

While we have emphasized the importance of convective influence in the TTL, it is important to note that uniform variations of the cold point temperature in the Tropics on both seasonal and interannual time scales appear due largely to changes in the large-scale ascent associated with the Brewer–Dobson circulation (Yulaeva et al. 1994; Reid and Gage 1996) and the quasi-biennial oscillation (QBO; Zhou et al. 2001; Randel et al. 2004). Figure 10 compares the equilibrium temperature profiles from the control experiment (dark), experiments w+3 (dashed) and SST+2 (light). We see that an increase in SST increases the height of the cold point but hardly changes its temperature (note that the effect on the TTL ozone field has been ignored here, which in the real atmosphere may produce further temperature changes). On the other hand, large-scale ascent leads to a higher and substantially colder cold point tropopause.

Results from this study suggest a picture relating large-scale ascent, deep convection, and the cold point tropopause that is similar to that of Reid and Gage (1996). In this picture, an enhanced large-scale ascent cools the entire TTL and lowers its static stability. This encourages deeper penetration by overshooting convection (all else being equal, a parcel can overshoot higher in a more weakly stratified environment). This effect is clearly evident in our simulations, and is also present in observational studies on both the annual time scale (Zhang 1993) and the QBO time scale (Collimore et al.

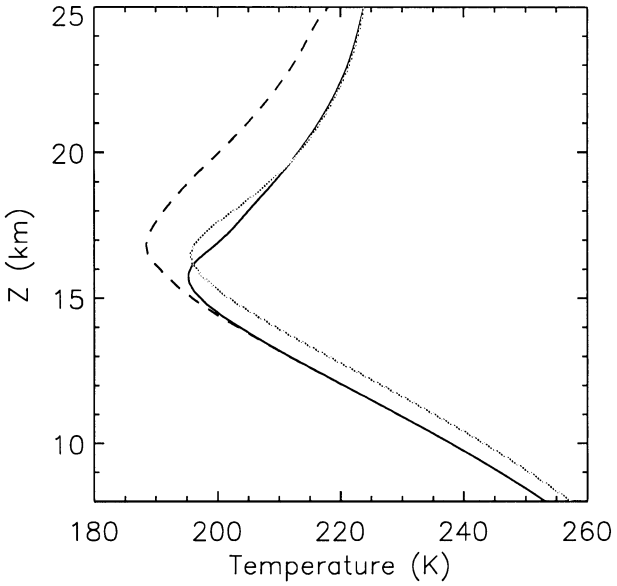

FIG. 10. The equilibrium temperature profiles from the control experiment (dark), experiment w+3 (dashed), and experiment SST+2 (light).

2003). The region of convective cooling is therefore shifted to a higher altitude as a response to the enhanced large-scale ascent. The shifted convective cooling further ''fine-tunes'' the temperature profile so that the cold point remains near the convective cooling maximum, which is now at a higher altitude. In a sense, cooling of the cold point is largely from the *direct* advective cooling associated with the large-scale ascent, while the higher cold point tropopause is realized *indirectly* via the effect of large-scale ascent on penetrative convection and hence convective cooling.

The view that the cold point tropopause is strongly tied to, rather than decoupled from, convection has implications for understanding dehydration processes in the TTL, which are important in regulating stratospheric humidity yet remain uncertain (Kley et al. 2000). Of central importance in the debate is whether convective or gradual processes are responsible for the dehydration. In the gradual scenario, the cold point tropopause is the fundamental dehydration agent that gradually freeze-dries the air as the air is advected across this temperature minimum (Holton and Gettelman 2001). Implicit in this scenario, however, is the assumption that convective influence is small at the cold point. Results from this study suggest that such an assumption is problematic; dehydration at the cold point cannot be taken for granted as gradual because the cold point itself is strongly tied to convective influence. The observed correlation between interannual variations of cold point tropopause temperature and stratospheric water vapor (Randel et al. 2004), therefore, should not be taken for granted as evidence for gradual dehydration. Instead of the cold point setting the water content by gradual dehydration, it is also possible that convection overshoots now reach higher so that convective dehydration is more effective. Such a distinction is of some importance because while they respond similarly on annual and interannual time scales, their response to longer-term global environmental changes can presumably be different. For instance, the convective dehydration process may be more susceptible to changes in aerosol concentrations (Sherwood 2002).

While we have chosen the simplified experimental settings to focus on the basic role of penetrative entrainment, and have not included, for instance, the diurnal cycle, mesoscale convective organization, and large-scale tropospheric circulation, our basic conclusions do not appear to depend on these simplifications. We have used a zero vertical wind shear profile to minimize gravity wave breaking. This choice helped to better isolate the effect of penetrative entrainment, and to demonstrate its potential role in the TTL heat balance. In the real atmosphere, gravity wave breaking and the breaking of large-scale equatorial waves represent another potential player in the TTL heat balance. Their importance, which presumably depends on the large-scale basic flow, is not addressed in this study, and warrants further investigation.

Observational confirmation for the climatological effects of diabatic convective cooling near the cold point tropopause is, unfortunately, rather difficult. It is very difficult to directly observe convective heat flux divergence to the degree of accuracy required here. A regional study is further complicated by the problem of separating adiabatic and diabatic effects and the effects of waves that propagate in and out of the region (Sherwood et al. 2003). There is evidence that diabatic cooling near the tropopause is needed over the Marine Continent to balance large-scale advective and clear-sky radiative effects (Sherwood and Dessler 2001). This was used as an indirect evidence for convective cooling. However, this evidence remains nondefinitive because thin cirrus over cold anvil clouds may provide an alternative source of the required diabatic cooling (Hartmann et al. 2001). How to confirm our model results observationally remains a challenge. On the other hand, as we illustrated in this paper, there are good dynamical reasons for the strong ties between convective cooling and the cold point, suggesting that these model results are nonetheless relevant to the real atmosphere.

Acknowledgments. We thank Marat Khairoutdinov for making the SAM model available, Peter Blossey and Marc Michelsen for helping with the computation, Andy Dessler for helpful discussions, and Steve Sherwood and one anonymous reviewer for careful and constructive reviews. Kuang was supported by a NOAA climate and global change postdoctoral fellowship. Bretherton was supported by NASA Grant NAGS5-10624.

REFERENCES

Collimore, C. C., D. W. Martin, M. H. Hitchman, A. Huesmann, and D. E. Waliser, 2003: On the relationship between the QBO and tropical deep convection. *J. Climate,* **16,** 2552–2568.

Deardorff, J. W., G. E. Villis, and G. H. Stockton, 1980: Laboratory studies of the entrainment zone of a convectively mixed layer. *J. Fluid Mech.,* **100,** 41–64.

Folkins, I., M. Loewenstein, J. Podolske, S. J. Oltmans, and M. Proffitt, 1999: A barrier to vertical mixing at 14 km in the tropics: Evidence from ozonesondes and aircraft measurements. *J. Geophys. Res.,* **104D,** 22 095–22 102.

Gettelman, A., M. L. Salby, and F. Sassi, 2002: Distribution and influence of convection in the tropical tropopause region. *J. Geophys. Res.,* **107D,** 4080, doi:10.1029/2001JD001048.

Hartmann, D. L., J. R. Holton, and Q. Fu, 2001: The heat balance of the tropical tropopause, cirrus, and stratospheric dehydration. *Geophys. Res. Lett.,* **28,** 1969–1972.

Holton, J. R., and A. Gettelman, 2001: Horizontal transport and the dehydration of the stratosphere. *Geophys. Res. Lett.,* **28,** 2799–2802.

Johnson, R. H., and D. C. Kriete, 1982: Thermodynamic and circulation characteristics of winter monsoon tropical mesoscale convection. *Mon. Wea. Rev.,* **110,** 1898–1911.

Khairoutdinov, M. F., and D. A. Randall, 2003: Cloud resolving modeling of the ARM summer 1997 IOP: Model formulation, results, uncertainties, and sensitivities. *J. Atmos. Sci.,* **60,** 607–625.

Kiehl, J. T., J. J. Hack, G. B. Bonan, B. A. Boville, D. L. Williamson, and P. J. Rasch, 1998: The National Center for Atmospheric Research Community Climate Model: CCM3. *J. Climate,* **11,** 1131–1149.

Kley, D., J. M. Russell III, and C. Phillips, Eds., 2000: Assessment of upper tropospheric and stratospheric water vapour. WMO Tech. Doc. 1043, 312 pp.

Lane, T. P., R. D. Sharman, T. L. Clark, and H. M. Hsu, 2003: An investigation of turbulence generation mechanisms above deep convection. *J. Atmos. Sci.,* **60,** 1297–1321.

Matcheva, K. I., and D. F. Strobel, 1999: Heating of Jupiter's thermosphere by dissipation of gravity waves due to molecular viscosity and heat conduction. *Icarus,* **140,** 328–340.

Mote, P. W., and Coauthors, 1996: An atmospheric tape recorder: The imprint of tropical tropopause temperatures on stratospheric water vapor. *J. Geophys. Res.,* **101D,** 3989–4006.

Randel, W. J., F. Wu, S. J. Oltmans, K. Rosenlof, and G. E. Nedoluha, 2004: Interannual changes of stratospheric water vapor and correlations with tropical tropopause temperatures. *J. Atmos. Sci.,* **61,** 2133–2148.

Reid, G. C., and K. S. Gage, 1996: The tropical tropopause over the western Pacific: Wave driving, convection, and the annual cycle. *J. Geophys. Res.,* **101D,** 21 233–21 241.

Salby, M., F. Sassi, P. Callaghan, W. Read, and H. Pumphrey, 2003: Fluctuations of cloud, humidity, and thermal structure near the tropical tropopause. *J. Climate,* **16,** 3428–3446.

Sherwood, S., 2002: A microphysical connection among biomass burning, cumulus clouds, and stratospheric moisture. *Science,* **295,** 1272–1275.

——, and A. E. Dessler, 2001: A model for transport across the tropical tropopause. *J. Atmos. Sci.,* **58,** 765–779.

——, T. Horinouchi, and H. A. Zeleznik, 2003: Convective impact on temperatures observed near the tropical tropopause. *J. Atmos. Sci.,* **60,** 1847–1856.

Thuburn, J., and G. C. Craig, 2002: On the temperature structure of the tropical substratosphere. *J. Geophys. Res.,* **107D,** 4017, doi:10.1029/2001JD000448.

Tompkins, A. M., and G. C. Craig, 1998: Radiative–convective equilibrium in a three-dimensional cloud-ensemble model. *Quart. J. Roy. Meteor. Soc.,* **124,** 2073–2097.

Webster, P. J., and R. Lukas, 1992: TOGA COARE: The Coupled Ocean–Atmosphere Response Experiment. *Bull. Amer. Meteor. Soc.,* **73,** 1377–1416.

Yulaeva, E., J. R. Holton, and J. M. Wallace, 1994: On the cause of the annual cycle in tropical lower-stratospheric temperatures. *J. Atmos. Sci.,* **51,** 169–174.

Zhang, C., 1993: On the annual cycle in highest, coldest clouds in the tropics. *J. Climate,* **6,** 1987–1990.

Zhou, X. L., M. A. Geller, and M. H. Zhang, 2001: Tropical cold point tropopause characteristics derived from ECMWF reanalyses and soundings. *J. Climate,* **14,** 1823–1838.